J. Phys. G: Nucl. Part. Phys. **22** (1996) 1483–1495. Printed in the UK

Cross section, spin distribution and mean spin analysis of low-energy heavy-ion fusion by closed formulae

Basudeb Sahu† and C S Shastry‡

† Department of Physics, Ravenshaw College, Cuttack 753 003, India
‡ Department of Physics, North Eastern Hill University, Shillong 793 022, India

Received 31 January 1996, in final form 12 June 1996

Abstract. In this paper, we analyse the fusion cross sections (σ_F), partial-wave fusion cross section (σ_F^l) and mean angular momenta $\langle l \rangle$ of heavy-ion (HI) fusion reactions around the Coulomb barrier for a number of pairs of colliding nuclei. This is done by first formulating expressions for σ_F in closed forms. These expressions incorporate only the general characteristics, namely radius, height and curvature of the s-wave potential barrier. The formulation is based on our earlier effective fusion barrier (EFB) transmission model. The values of σ_F, σ_F^l and $\langle l \rangle$ calculated around the Coulomb barrier using our expressions provide good fits to the corresponding experimental results in the cases of several HI systems, namely $^{64}Ni + {}^{92,96}Zr$, $^{64}Ni + {}^{100}Mo$ and $^{16}O + {}^{166}Er$.

1. Introduction

The fusion of two nuclei at bombarding energy in the vicinity of the Coulomb barrier is one of the important mechanisms of heavy-ion collisions (HICs). We find several model dependent approaches in the literature [1, 2] to estimate the cross section of fusion σ_F starting from the simple barrier penetration model (BPM) to more sophisticated approaches such as coupled-channel (CC) calculations. However, the experimental σ_F data for all kinds of heavy-ion (HI) pairs have not been explained fully by any of these attempts in the whole energy range starting from the below-barrier to the far-above-barrier region in one go. Particularly in the sub-barrier region, the experimental results of σ_F in the cases of heavier pairs are underestimated by most of the calculations.

Furthermore, a deeper look at the mechanism of fusion reveals that the total σ_F is the sum of the contributions from different angular momentum ($l\hbar$) trajectories in the reaction process. This fact indicates that σ_F may have a coherent relationship with the corresponding spin distribution or partial-wave fusion cross section σ_F^l obtained for various partial waves l. Any model describing fusion should, therefore, explain the cross section and spin involved in the process consistently. In view of this, information (experimental) about the angular momenta involved in the fusion process is very important when probing the physical validity of the concepts incorporated in various models used for the estimate of σ_F. In recent times, along with σ_F, measured data of σ_F^l and mean spin or average angular momenta $\langle l \rangle$ for nucleus–nucleus fusion have started to become available [3–5]. A most recent review in [6] and the analysis of Stefanini [5] show that although the standard CC calculations [7, 8] are successful in reproducing the σ_F and $\langle l \rangle$ data in the cases of light and/or very asymmetric heavy pairs of nuclei, they fail to do so in the cases of more heavy and nearly symmetric systems such as $^{64}Ni + {}^{92,96}Zr$, $^{64}Ni + {}^{100}Mo$ etc. Like the BPM [9] or the Wong [10]

0954-3899/96/101483+13$19.50

formulae, the CC calculations are found to give values of both σ_F and $\langle l \rangle$ with much lower values than those obtained by experiments, particularly in the below-barrier region of energy. Also, it is seen in the literature [5] that the Wong formula [10] needs further drastic modifications for explaining σ_F and σ_F^l data simultaneously in cases such as $^{64}Ni + ^{92,96}Zr$.

In this paper, we discuss this problem of sub-barrier enhancement of σ_F and $\langle l \rangle$ within the framework of a macroscopic approach maintaining a consistency between the fusion cross section and spin distribution.

Generally, the fusion of heavy ions at low bombardment energies is governed by the quantum mechanical penetration through the Coulomb plus centrifugal barrier. Recently we have developed [11] a simple formulation for the estimate of σ_F in HIC which is consistent with the concept of one-dimensional BPM and the direct reaction model (DRM) [12] of fusion. This model has been named as an effective fusion barrier (EFB) transmission model. The basic idea behind this model can be described as follows. If one accepts the concepts of the DRM of fusion developed by Udagawa *et al* [12] that fusion takes place due to absorption in the region

$$r \leqslant R_F = r_F(A_1^{1/3} + A_2^{1/3})$$

r_F being the fusion radius parameter for the colliding nuclei with mass numbers A_1 and A_2, then within the framework of the BPM picture one can visualize that the fusion of two interacting nuclei takes place when they penetrate into the sphere $r = R_F$. That is, according to this concept, once the colliding nuclei have centre-of-mass separation $r < R_F$, fusion takes place. This is also clear from the fact that the wavefunction gets drastically attenuated for $r < R_F$ due to a strong absorptive potential. Thus the transmission into this sphere is the primary process involved in the fusion mechanism which is consistent with the observation in [13] regarding fusion. This model is able to explain in a neat way σ_F around the Coulomb barrier in the cases of several HI pairs [11].

In this paper, we first generalize our previous EFB model formulation and obtain expressions for T_l at E_{cm} both below and above the barrier in a unified way following a neat mathematical procedure given by Farina [14]. We then derive the final expressions for σ_F in closed form which are found to be different from the corresponding expressions given by Wong [10]. The formulae for σ_F and σ_F^l are expressed in terms of the fusion barrier parameters, namely the radius, height and curvature of the s-wave barrier. In the application of the present formulae to fit the fusion data for different nucleus–nucleus systems, the only parameter that needs to be varied is R_F. In order to make the fusion process consistent with the scattering process, it is emphasized that R_F should be very close to $R_B^{(OMP)}$, which is the position of the s-wave barrier obtained by using the optical model potential (OMP) parameters which describe scattering data. This is important in view of the fact that for strong absorption the barrier position has to be reached, in other words, $R_B^{(OMP)}$ should be the entry point for the onset of fusion. This is consistent with the fact that in the exterior region $r > R_B^{(OMP)}$, generally, the contribution to fusion can be expected to be small; and the relatively weak absorption in the outside region will contribute more to other types of reactions. This view is reflected in the traditional assumption that the fusion occurs mostly in a region interior to the Coulomb barrier. Consequently, the introduction of a critical fusion radius parameter around the barrier position is a common feature of our model, the DRM [12] and CC calculations [15]. Furthermore, in connection with the onset of fusion at large distances, mention should be made of the work of Marten and Fröbrich [16] in which fusion is determined at large distances due to the frictional effects in the entrance channel.

In our earlier works [11], we have calculated σ_F and obtained good fits with the corresponding experimental σ_F data in the cases of several HI systems, namely $^{16}O + ^{27}Al$,

$^{16}O + {}^{40}Ca$, $^{16}O + {}^{148,152}Sm$, $^{40}Ca + {}^{40,44}Ca$, $^{40}Ar + {}^{122}Sn$ and $^{58}Ni + {}^{58,64}Ni$ around the Coulomb barrier using the EFB model. Using the present unified version of this model, we calculate σ_F, σ_F^l and $\langle l \rangle$ for the systems $^{64}Ni + {}^{92,96}Zr$, $^{64}Ni + {}^{100}Mo$ and $^{16}O + {}^{166}Er$ for which the experimental data of both σ_F and $\langle l \rangle$ are available in the literature at energies around the Coulomb barrier. Good fits between the respective calculated and measured data of these quantities are obtained simultaneously.

The paper is organized in the following way. The generalization of the EFB model and the deduction of closed form expressions for σ_F, σ_F^l and $\langle l \rangle$ are described in section 2. In section 3, the results of numerical calculations of σ_F, σ_F^l and $\langle l \rangle$ for various nucleus–nucleus systems are presented and compared with the corresponding results obtained from experiments and other theoretical approaches. We summarize our findings in section 4.

2. General expressions for T_l in the EFB model

In the EFB transmission model elaborated in [11], the effective barrier for the lth partial wave is assumed to be

$$V_{EFB}(l,r) = \begin{cases} V_N(r) + V_C(r) + V_l(r) & \text{if } r \geqslant R_F \\ 0 & \text{if } r < R_F \end{cases} \tag{1}$$

where $V_l = (\hbar^2/2\mu)[l(l+1)/r^2]$ with μ denoting reduced mass, $V_N(r)$ is the real part of the heavy-ion OMP and $V_C(r)$ is the usual form of the nucleus–nucleus electrostatic potential with radius parameter r_C. Assuming that the fusion is initiated between the two nuclei when they penetrate into the sphere of radius R_F, the effective barrier described by equation (1) has to be transmitted (or tunnelled through) in the lth partial wave for the fusion to take place. Kittl and Testoni [17] have also recognized that a sharp cut-off-type potential is feasible for describing fusion within some radius. Furthermore, the effect of channel couplings in the process of fusion can be reproduced by one-channel tunnelling through a single barrier obtained by considering a large depth (V_0) and small diffuseness parameter (a_v) in the Woods–Saxon form of the optical model nuclear potential [3, 15]. This would lead to a steep and thinner effective barrier similar to that considered in the EFB model represented by equation (1) in the extreme limit. In [11], we have obtained an expression for the coefficient of the transmitted wave T_l within the framework of the quasi-classical approximation (WKB) for a given l at an incident energy $E_{cm} > V_{EB}^l$. Let it be denoted as $T_l^{(AB)}$ in this above-barrier (AB) situation and expressed as

$$T_l^{(AB)} = \left. \frac{4k\kappa(l,r)}{[k+\kappa(l,r)]^2 + [\kappa'(l,r)/(2\kappa(l,r))]^2} \right|_{r=R_F} \qquad E_{cm} > V_{EB}^l \tag{2}$$

where

$$k^2 = \frac{2\mu E_{cm}}{\hbar^2} \qquad \kappa^2(l,r) = \frac{2\mu}{\hbar^2}[E_{cm} - V_{EFB}(l,r)]. \tag{3}$$

Here

$$V_{EB}^l = V_{EB}^0 + \frac{\hbar^2 l(l+1)}{2\mu R_F^2}$$

is the height of the effective barrier at $r = R_F$ in the lth partial wave with V_{EB}^0 being the corresponding result for the s-wave. Prime denotes differentiation with respect to r.

When $E_{cm} < V_{EB}^l$, we express $\kappa(l,r) = -i\tilde{\kappa}(l,r)$ in the region $R_F \leqslant r < r_1$, where r_1 denotes the outermost turning point and $[\tilde{\kappa}(l,r)]^2 = -[\kappa(l,r)]^2$. Following

the mathematical procedure given in [14], within the first-order WKB approximation, we obtain, besides equation (2), the T_l below the barrier as

$$T_l^{(\mathrm{SB})} = \left.\frac{4k\tilde{\kappa}(l,r)\theta^2}{k^2 + [\tilde{\kappa}(l,r) - [\tilde{\kappa}'(l,r)/(2\tilde{\kappa}(l,r))]]^2}\right|_{r=R_\mathrm{F}} \qquad E_\mathrm{cm} < V_\mathrm{EB}^l \tag{4}$$

where $\theta = \exp[-\int_{R_\mathrm{F}}^{r_1} \tilde{\kappa}(l,r)\,\mathrm{d}r]$. Here SB indicates the sub-barrier situation. It may be pointed out that the expressions given by (2) and (4) have some structural similarity. These expressions are deduced using the WKB formulation and hence will not be fully valid for a few partial waves for which $E_\mathrm{cm} \simeq V_\mathrm{EB}^l$ due to the fact that both turning points become very close to each other. At these turning points the WKB wavefunction, as discussed in detail in [18], substantially deviates from the exact wavefunction, but it is highly accurate in the region away from the turning points. We refer to this point again in section 3.

2.1. Closed formulae for σ_F

The partial-wave expansion for σ_F is given by

$$\sigma_\mathrm{F} = \frac{\pi}{k^2}\sum_{l=0}^{\infty}(2l+1)T_l \tag{5}$$

where T_l is obtained from equations (2) and (4). Further simplification of equation (5) is now made, as in [10], by considering the leading terms of the Poisson sum formula to arrive at a closed formula for σ_F.

For a given incident energy $E_\mathrm{cm} > V_\mathrm{EB}^0$, the grazing partial wave l_g is obtained from the condition $\kappa(l = l_\mathrm{g}, r = R_\mathrm{F}) = 0$ where $\kappa(l,r)$ is given by equation (3). For the lower set of partial waves $0 \leqslant l < l_\mathrm{g}$, we have an AB situation with $E_\mathrm{cm} > V_\mathrm{EB}^l$. For the remaining partial waves $l \geqslant l_\mathrm{g}$, this comes under an SB situation having $E_\mathrm{cm} \leqslant V_\mathrm{EB}^l$. However, for $E_\mathrm{cm} \leqslant V_\mathrm{EB}^0$ it is an SB situation for all ls.

Thus for certain $E_\mathrm{cm} > V_\mathrm{EB}^0$, σ_F of equation (5) can be expressed as

$$\sigma_\mathrm{F} = \frac{\pi}{k^2}\sum_{l=0}^{l_\mathrm{g}}(2l+1)T_l^{(\mathrm{AB})} + \frac{\pi}{k^2}\sum_{l_\mathrm{g}}^{\infty}(2l+1)T_l^{(\mathrm{SB})} = \sigma_\mathrm{F}^{(1)} + \sigma_\mathrm{F}^{(2)} \tag{6}$$

$$\sigma_\mathrm{F}^{(1)} = \frac{\pi}{k^2}\sum_{l=0}^{l_\mathrm{g}}(2l+1)T_l^{(\mathrm{AB})} \tag{7}$$

$$\sigma_\mathrm{F}^{(2)} = \frac{\pi}{k^2}\sum_{l_\mathrm{g}}^{\infty}(2l+1)T_l^{(\mathrm{SB})}. \tag{8}$$

The expression (7) for $\sigma_\mathrm{F}^{(1)}$ is further simplified as follows.

With the assumption that $\kappa'(l,r) \simeq 0$ at $r = R_\mathrm{F} \simeq R_\mathrm{B}^{(\mathrm{OMP})}$, $T_l^{(\mathrm{AB})}$ given by equation (2) reduces to

$$T_l^{(\mathrm{AB})} \simeq \left.\frac{4k\kappa(l,r)}{[k+\kappa(l,r)]^2}\right|_{r=R_\mathrm{F}}. \tag{9}$$

Using equation (9) in equation (7) and replacing the sum over l by integration, we obtain the following closed expression for $\sigma_\mathrm{F}^{(1)}$:

$$\sigma_\mathrm{F}^{(1)} = 8\pi R_\mathrm{F}^2[(1+\alpha) - 2\ln(1+\alpha) - (1+\alpha)^{-1}] \qquad E_\mathrm{cm} > V_\mathrm{EB}^0 \tag{10}$$

where $\alpha = (1 - (V_\mathrm{EB}^0/E_\mathrm{cm}))^{1/2}$ and is real for $E_\mathrm{cm} > V_\mathrm{EB}^0$. It is clear from equation (10) that for $E_\mathrm{cm} \gg V_\mathrm{EB}^0$, $\alpha \simeq 1$ and we have $\sigma_\mathrm{F}^{(1)} \simeq \pi R_\mathrm{F}^2$.

In the SB situation, $T_l^{(\mathrm{SB})}$ given by equation (4) reduces to

$$T_l^{(\mathrm{SB})} \simeq \frac{4E_{\mathrm{cm}}^{1/2}}{V_{\mathrm{EB}}^0}[V_{\mathrm{EB}}^l - E_{\mathrm{cm}}]^{1/2}\theta^2. \tag{11}$$

This is obtained by assuming that (i) $\tilde{\kappa}'(l,r) \simeq 0$ at $r = R_{\mathrm{F}} \simeq R_{\mathrm{B}}^{(\mathrm{OMP})}$ and (ii) $V_{\mathrm{EB}}^0 \gg \hbar^2 l(l+1)/2\mu R_{\mathrm{F}}^2$ for most of the significant ls contributing to sub-barrier fusion. Furthermore, we evaluate the integral in the expression for θ by considering the total effective potential $V_{\mathrm{EFB}}(l,r)$ as parabolic and obtain

$$\theta^2 \simeq \exp[-(V_{\mathrm{EB}}^l - E_{\mathrm{cm}})/\Delta e] \tag{12}$$

where $\Delta e = \hbar w_{\mathrm{F}}/\pi$ with

$$w_{\mathrm{F}}^2 = \left[-\frac{1}{\mu}\frac{\mathrm{d}^2 V_{\mathrm{EFB}}(l,r)}{\mathrm{d}r^2}\right]$$

calculated at $r = R_{\mathrm{F}}$. The fusion radius R_{F} and the curvature factor w_{F} could be assumed to be independent of l for potentials in HI systems. Using these assumptions and expression (11) along with expression (12) in equation (5), we obtain in the SB energy region ($E_{\mathrm{cm}} \leqslant V_{\mathrm{EB}}^0$) the following expressions for σ_{F} in closed form after integration over l as before:

$$\sigma_{\mathrm{F}} = G\frac{\Gamma(\frac{3}{2},\beta)}{E_{\mathrm{cm}}^{1/2}} \qquad E_{\mathrm{cm}} \leqslant V_{\mathrm{EB}}^0 \tag{13}$$

where $G = 4\pi R_{\mathrm{F}}^2(\Delta e)^{3/2}/V_{\mathrm{EB}}^0$, $\beta = (V_{\mathrm{EB}}^0 - E_{\mathrm{cm}})/\Delta e$ and $\Gamma(\frac{3}{2},\beta)$ is the incomplete gamma function.

Using the standard properties of $\Gamma(\frac{3}{2},\beta)$, we simplify expression (13) as follows. For E_{cm} below but close to V_{EB}^0 such that $\beta \leqslant 1$ [19], we have

$$\Gamma(\tfrac{3}{2},\beta) \simeq \frac{\sqrt{\pi}}{2} - 2.9883\frac{\beta^{1/2}}{(3+\beta)} + \beta^{1/2}\exp(-\beta). \tag{14}$$

With this, equation (13) reduces to

$$\sigma_{\mathrm{F}} \simeq \frac{4\pi R_{\mathrm{F}}^2(\Delta e)^{3/2}}{V_{\mathrm{EB}}^0 E_{\mathrm{cm}}^{1/2}}\left[\frac{\sqrt{\pi}}{2} - 2.9883\frac{\beta^{1/2}}{(3+\beta)} + \beta^{1/2}\exp(-\beta)\right] \qquad \beta \leqslant 1. \tag{15}$$

Furthermore, in the region far below the barrier where $\beta > 1$ [19], one can take

$$\Gamma(\tfrac{3}{2},\beta) \simeq \left(1 + \frac{1}{2\beta}\right)\beta^{1/2}\exp(-\beta). \tag{16}$$

Using this in equation (13), we find

$$\sigma_{\mathrm{F}} \simeq \frac{4\pi R_{\mathrm{F}}^2(\Delta e)^{3/2}}{V_{\mathrm{EB}}^0 E_{\mathrm{cm}}^{1/2}}\left[1 + \frac{1}{2\beta}\right]\beta^{1/2}\exp(-\beta) \qquad \beta > 1. \tag{17}$$

At $E_{\mathrm{cm}} = V_{\mathrm{EB}}^0$ where $\beta = 0$, we find from equation (15) that

$$\sigma_{\mathrm{F}} = \sigma_{\mathrm{F}}^{(2)} = 2R_{\mathrm{F}}^2\left(\frac{\pi\Delta e}{E_{\mathrm{cm}}}\right)^{3/2}. \tag{18}$$

This situation is similar to the case at $E_{\mathrm{cm}} = V_{\mathrm{EB}}^{l_{\mathrm{g}}}$ where $l_{\mathrm{g}} \geqslant 0$. Hence, $\sigma_{\mathrm{F}}^{(2)}$ given by equation (8) could be expressed as that in equation (18).

Thus, at a given energy E_{cm} the value of total σ_{F} is estimated in the AB situation ($E_{\mathrm{cm}} > V_{\mathrm{EB}}^0$) by using equations (10) and (18) in equation (6) and in the SB case ($E_{\mathrm{cm}} \leqslant V_{\mathrm{EB}}^0$) by using equations (15) and (17).

2.2. Spin distribution and average angular momenta

The energy dependence of σ_F determines the spin distribution uniquely. In this regard, we note that one can use the procedure given in [5] to get σ_F^l from σ_F. Then the expression for σ_F^l becomes

$$\sigma_F^l = \frac{(2l+1)}{k^2R^2}\left[E'\left.\frac{d\sigma_F}{dE_{cm}}\right|_{E_{cm}=E'} + \sigma_F(E_{cm}=E')\right] \tag{19}$$

where $E' = E_{cm} - E_{rot}$, $E_{rot} = (\hbar^2/2\mu)[l(l+1)/R^2]$ and $k^2 = (2\mu E_{cm})/\hbar^2$. Here R is the centre-to-centre mass separation and E_{rot} stands for rotational energy in a given trajectory specified by the partial wave l. Equation (19) is a convenient formula to find σ_F^l. Then the average angular momenta $\langle l\rangle$ at certain energy E_{cm} is given by

$$\langle l\rangle = \frac{\sum_{l=0}^{\infty} l\sigma_F^l}{\sigma_F}. \tag{20}$$

For a given incident energy $E_{cm} > V_{EB}^0$, one encounters two situations: (i) $E' = (E_{cm} - E_{rot}) > V_{EB}^0$ for $l < l_g$ and (ii) $E' \leqslant V_{EB}^0$ for $l \geqslant l_g$. However, for $E_{cm} \leqslant V_{EB}^0$ it is seen that $E' \leqslant V_{EB}^0$ for all ls. Keeping this in view, we derive the spin distribution σ_F^l and the average angular momenta $\langle l\rangle$ from the closed expressions for σ_F deduced earlier and equations (19) and (20). The results are:

(i)

$$\sigma_F^l(E_{cm}) = \left(\frac{2l+1}{k^2R_F^2}\right) \times \left(\frac{AV_{EB}^0}{2E'}\frac{\alpha'}{(1+\alpha')^2} + A[(1+\alpha') - 2\ln(1+\alpha') - (1+\alpha')^{-1}] + \frac{B}{2(E')^{3/2}}\right) \tag{21}$$

where

$$E' = (E_{cm} - E_{rot}) > V_{EB}^0 \qquad E_{rot} = (\hbar^2/2\mu)[l(l+1)/R_F^2]$$
$$\alpha' = \left(1 - \frac{V_{EB}^0}{E'}\right)^{1/2} \qquad A = 8\pi R_F^2 \qquad B = 2(\pi\Delta e)^{3/2}R_F^2.$$

(ii)

$$\sigma_F^l(E_{cm}) = G\left(\frac{2l+1}{k^2R_F^2}\right)\left[\frac{\Gamma(\frac{3}{2},\beta')}{2(E')^{1/2}} + \frac{(E')^{1/2}(\beta')^{1/2}}{\Delta e}\exp(-\beta')\right] \qquad E' \leqslant V_{EB}^0 \tag{22}$$

where $\beta' = (V_{EB}^0 - E')/\Delta e$. The incomplete gamma function $\Gamma(\frac{3}{2},\beta')$ is estimated as in equations (14) and (16) for the values of β' in the two limiting situations. These equations (21) and (22) provide simple and convenient expressions for σ_F^l on the basis of equation (19).

Using the above formulations we explain the experimental data of σ_F, σ_F^l and $\langle l\rangle$ in the cases of various nucleus–nucleus systems in the following section.

3. Numerical results and discussion

In this section, we demonstrate the applicability of our above formulation through simultaneous analysis of the experimental data for σ_F, σ_F^l and $\langle l\rangle$ in the cases of several HI pairs such as ^{64}Ni + ^{92,96}Zr, ^{64}Ni + ^{100}Mo and ^{16}O + ^{166}Er over a wide range of energies around the Coulomb barrier and compare our results with those of CC calculations. We

Table 1. Systems, R_F, V_{EB}^0, $\hbar w_F$ and r_0 used in the calculation and the barrier radius $R_B = 1.07(A_1^{1/3} + A_2^{1/3}) + 2.72$ fm.

System	$\hbar w_F$ (MeV)	V_{EB}^0 (MeV)	r_0 (fm)	R_F (fm)	R_B (fm)
$^{64}Ni + ^{92}Zr$	4.33	131.7	1.04	11.57	11.82
$^{64}Ni + ^{96}Zr$	4.21	129.2	1.06	11.81	11.89
$^{64}Ni + ^{100}Mo$	4.23	134.0	1.07	11.96	11.96
$^{16}O + ^{166}Er$	4.9	64.6	1.09	11.45	11.29

denote the results of σ_F of the present calculation by σ_F^{closed} and the corresponding results from experiment by σ_F^{expt}.

It is well known that there are a number of OMP parameter sets which can almost equally fit the same elastic scattering angular distribution data. Therefore, we prefer to use 'global' expressions for R_F, V_{EB}^0 and w_F deduced using a global HI potential [20, 21]:

$$R_F = [r_0(A_1^{1/3} + A_2^{1/3}) + 2.72] \text{ fm} \tag{23}$$

$$V_{EB}^0 = \frac{Z_1 Z_2 e^2}{R_F}\left(1 - \frac{a}{R_F}\right) \tag{24}$$

$$(\hbar w_F)^2 = \frac{Z_1 Z_2 e^2 \hbar^2}{\mu R_F^2}\left(\frac{1}{a} - \frac{2}{R_F}\right) \tag{25}$$

where $a = 0.63$ fm and $r_0 = 1.07$ fm [20]. Here μ indicates the reduced mass and A_i, Z_i, $i = 1, 2$, denote the mass number and proton number of the colliding nuclei. In the application of our formula, we slightly vary the radius parameter r_0 around the global value (1.07 fm) in individual cases for a better fit to σ_F^{expt}. Thus R_F is the only variable parameter used in our calculation as V_{EB}^0 and w_F are expressed in terms of R_F and fixed a in equations (24) and (25). In view of the success of calculated σ_F, σ_F^l and $\langle l \rangle$ values we believe the use of R_F as an adjustable parameter implicitly incorporates the net effect of the microscopic processes such as coupled channels, barrier distributions etc. Similar observation regarding shifting of fusion radius to incorporate channel-coupling effects is pointed out in [22] (also see [3, 13, 15]). In table 1 we list the nucleus–nucleus systems studied along with the results of R_F, V_{EB}^0, $\hbar w_F$ and r_0 used in the present calculation. A study of this table reveals that:

(i) $r_0 = 1.07 \pm 0.03$ fm. It is seen that the values of R_F obtained using these values of r_0 in the cases of different systems are, in general, close to the respective Coulomb barrier radii $R_B^{(OMP)}$. For example, in the case of $^{64}Ni + ^{100}Mo$ the barrier is situated at $R_B^{(OMP)} = 11.4$ fm with height $V_B^{(OMP)} = 138.6$ MeV which are obtained by using the OMP parameters $V_0 = 178$ MeV, $r_v = 1.087\,27$ fm and $a_v = 0.707$ fm [3]. Thus, in this case the value of R_F (= 11.96 fm (see table 1)) used by us is close to $R_B^{(OMP)}$. In the cases of light HI systems (not included in table 1) r_0 is found to be closer to unity giving $R_F \leqslant R_B^{(OMP)}$. These results corroborate the general assumption that fusion processes are spatially localized inside the Coulomb barrier region [2, 15].

(ii) $\hbar w_F \sim 4$ MeV. This result is also consistent with the typical values of $\hbar w$ for HI pairs found in the literature [21].

In figures 1–3, we compare the results of σ_F^{closed} of present calculation with σ_F^{expt} at several E_{cm} around the Coulomb barrier for the $^{64}Ni + ^{92,96}Zr$ (figure 1), $^{64}Ni + ^{100}Mo$ (figure 2) and $^{16}O + ^{166}Er$ (figure 3) systems. In each figure σ_F^{closed} is represented by full

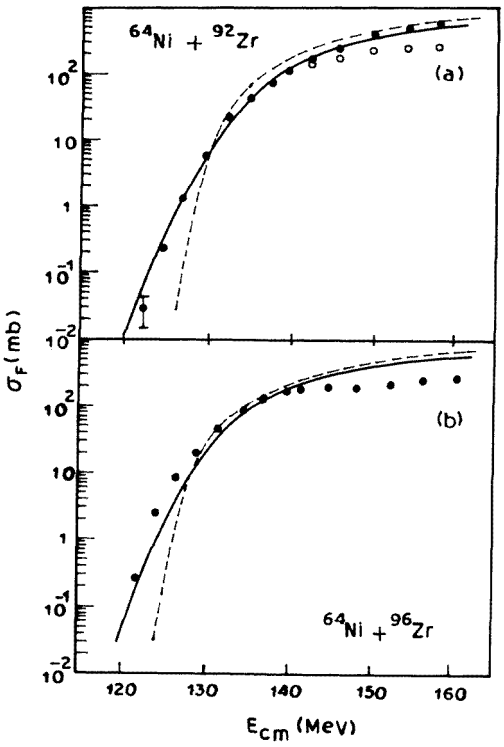

Figure 1. Variation of fusion cross section σ_F as a function of E_{cm} for $^{64}Ni + ^{92,96}Zr$ systems. The full curves represent σ_F^{closed} of the present calculation. The experimental data and the results of CC calculations represented by broken curves have been taken from [5]. Measured data are shown as open circles (ER) and full circles (ER + fission) in the upper part and by full circles (ER) in the lower part of the figure.

curves. It is seen that the fit of σ_F^{closed} to σ_F^{expt} is quite good in general. Coming to the individual cases we may point out that in the case of $^{64}Ni + ^{96}Zr$ in figure 1(*b*) the σ_F^{expt} data (full circles) correspond to only an evaporation residue (ER) cross section [5]. When the measured fission cross section is added to these ER results, the resulting σ_F can be expected to agree with the the results of our calculation (full curve) more closely as in figure 1(*a*) for $^{64}Ni + ^{92}Zr$. Also in figure 1 we show the results of CC calculations by a broken curve which underpredicts the cross section below the barrier [5]. A similar problem of underprediction of σ_F^{expt} is found in $^{64}Ni + ^{100}Mo$ (figure 2) by CC calculations. However, our results shown by the full curve systematically remove this problem in all these cases. Even in the case of $^{16}O + ^{166}Er$ (figure 3(*a*)), where the CC model is successful, our results are also equally good.

3.1. Spin distribution and mean spin

We now analyse the data of σ_F^l and the corresponding $\langle l \rangle$ involved in the fusion process. These data for the systems $^{64}Ni + ^{92}Zr$ and $^{64}Ni + ^{96}Zr$ are obtained from the paper [5]. We obtain the corresponding results from our present formulae (20)–(22). In figure 4 the variation of σ_F^l with l at fixed energy $E_{cm} = 138.8$ MeV for $^{64}Ni + ^{92}Zr$ and

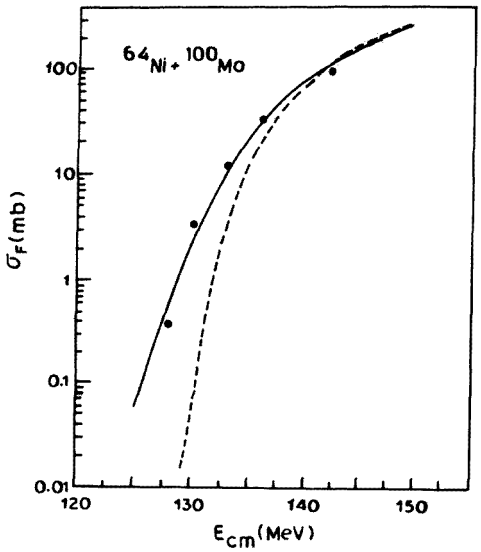

Figure 2. Same as figure 1 for the $^{64}\mathrm{Ni} + {}^{100}\mathrm{Mo}$ system. The full curves represent $\sigma_{\mathrm{F}}^{\mathrm{closed}}$. The results of CC calculations (broken curve) and experimental data (full circles) are obtained from [3].

$E_{\mathrm{cm}} = 139.5$ MeV for $^{64}\mathrm{Ni} + {}^{96}\mathrm{Zr}$ is shown. The full circles represent experimental results and the full curves represent our calculated results. As pointed out earlier, the WKB approach adopted by us is not appropriate for those partial waves for which $E_{\mathrm{cm}} \simeq V_{\mathrm{EB}}^{l}$. Due to this, σ_{F}^{l} for $l_{\mathrm{g}} - \Delta g < l < l_{\mathrm{g}} + \Delta g$, $\Delta g \simeq 1.5$ are evaluated by extrapolation and these results are shown by a dotted curve in figure 4. This is not unreasonable because the WKB approach, where applicable, gives a very good approximation to the exact wavefunction on either side of the turning point and deviation is appreciable only in the close vicinity of the turning point. This is elaborated in the work of More and Warren [18]. The matching between our calculated and experimental σ_{F}^{l} results is found to be quite good. Also the figure contains the values of σ_{F}^{l} (broken curve) obtained by adopting similar procedure for a modified Wong formula [5]. For the sake of completeness, we give below the Wong formula for σ_{F}

$$\sigma_{\mathrm{F}} = \pi R_{\mathrm{B}}^{2} \frac{\Delta E}{E_{\mathrm{cm}}} \ln[1 + \exp((E_{\mathrm{cm}} - V_{\mathrm{B}})/\Delta E)]. \tag{26}$$

Here $\Delta E = \hbar w_{\mathrm{B}}/2\pi$ and R_{B}, V_{B} and w_{B} indicate the radius, height and curvature of the s-wave potential barrier, respectively. In order to obtain the fits (broken curves in figure 4) to the experimental σ_{F}^{l} it was found that the above formula needs further modification requiring the addition of another term $\exp[2\pi(E_{\mathrm{cm}} - V_{\mathrm{B}})/\hbar w_2]^2$ inside the log term in equation (26). However, the physical origin and significance of this term, as stated in [5], is not clear. This fact brings out clearly the merit and advantage of our approach. We have also successfully explained the σ_{F}^{l} against l data at different energies given in [3] for the $^{64}\mathrm{Ni} + {}^{100}\mathrm{Mo}$ system using our present formulation. This will be reported in another full paper.

The results of $\langle l \rangle$ corresponding to σ_{F} at various energies are analysed for $^{16}\mathrm{O} + {}^{166}\mathrm{Er}$ (figure 3(*b*)), $^{64}\mathrm{Ni} + {}^{92,96}\mathrm{Zr}$ (figure 5) and $^{64}\mathrm{Ni} + {}^{100}\mathrm{Mo}$ (figure 6) systems. Our results shown by full curves explain the data well throughout the energy region in all these cases. Particularly in the case of $^{16}\mathrm{O} + {}^{166}\mathrm{Er}$ and $^{64}\mathrm{Ni} + {}^{100}\mathrm{Mo}$, the fits are excellent. We may

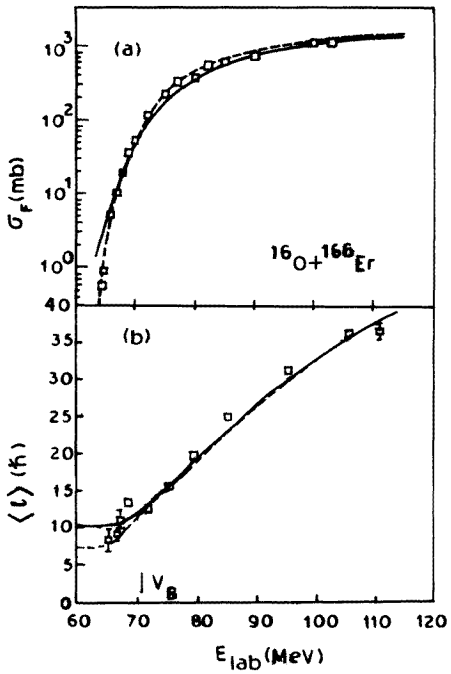

Figure 3. (*a*) Plot of σ_F as a function of laboratory energy E_{lab} for the $^{16}O+^{166}Er$ system. Full curve for σ_F^{closed} and broken curve for CC results. Experimental data (open squares) and CC results are obtained from [4]. (*b*) Variation of $\langle l \rangle$ as a function of E_{lab}. The full curve represents the results of the present calculation. The CC results (broken curve) and experimental data (open squares) are obtained from [4]. V_B indicates the Coulomb barrier height.

mention here that the system $^{64}Ni + ^{100}Mo$ has also been studied in [23, 24] for σ_F, σ_F^l and $\langle l \rangle$ using a model which considers ion deformations during the tunnelling process and energy dissipation. In these calculations the results of $\langle l \rangle$ are found to overestimate the corresponding $\langle l \rangle$ data in the above-barrier energy region. In figure 5 we see that our results (full curve) are more close to the data than the corresponding values of CC calculations in the lower energy region, whereas they merge with each other in the higher energy region with a satisfactory fit to the data, particularly in the case of $^{64}Ni + ^{96}Zr$ (figure 5(*a*)). Here also the present calculation is successful in explaining the data in the energy region where there is severe underprediction of $\langle l \rangle$ data by the CC calculations. In the case of $^{16}O+^{166}Er$ (figure 3(*b*)) both the CC calculation and our model are successful in explaining the $\langle l \rangle$ data remarkably well with a better fit in the latter case in the below-barrier energy region.

The set of expressions for σ_F, σ_F^l and $\langle l \rangle$ obtained in this paper using the unified mathematical approach [14] within the framework of the WKB approximation and EFB model [11] seem to provide remarkably successful formulae within the macroscopic approach for the analysis of HI fusion data. In our view, introduction of the concept of fusion resulting due to the tunnelling into the absorptive sphere $r < R_F$ with R_F as an adjustable parameter around the Coulomb barrier position seems to implicitly take into account the role of peripheral processes and varying barrier distribution in causing fusion

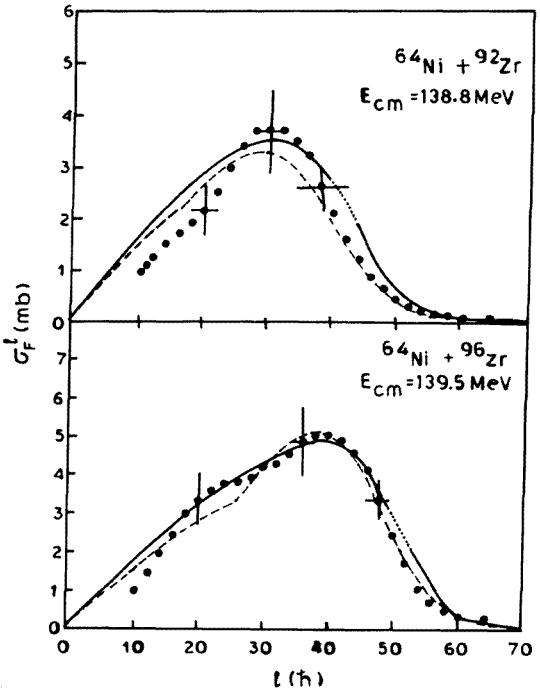

Figure 4. Spin distributions for ^{64}Ni + ^{92,96}Zr systems. Full curves represent results of the present calculation with the extrapolated results (see text) shown by dotted curves. The corresponding data (full circles) and the broken curves representing modified Wong results are obtained from [5].

[25]. One may note that the $\sigma_F^{(1)}$ given by equation (10) reduces to

$$\sigma_F^{(1)} \simeq \frac{8\pi R_F^2}{3}\left[1 - \frac{V_{EB}^0}{E_{cm}}\right]^{3/2} \tag{27}$$

when $E_{cm} \simeq V_{EB}^0$. This is significantly different from the two-parameter (R_{cr}, V_B) formula for σ_F in the l-space sharp-cut-off model given by

$$\sigma_F = \pi R_{cr}^2\left(1 - \frac{V_B}{E_{cm}}\right). \tag{28}$$

However, our expression (27) is interesting in the sense that it leads to the following expression for the second derivative of the function $E_{cm}\sigma_F$ with respect to E_{cm} for a single barrier:

$$\frac{d^2(E_{cm}\sigma_F)}{dE_{cm}^2} = \frac{2\pi R_F^2 (V_{EB}^0)^2}{E_{cm}^{5/2}(E_{cm} - V_{EB}^0)^{1/2}}. \tag{29}$$

This expression clearly shows the peak indicating the fusion barrier. We further note that there is provision in the present model to take into account the barrier distribution by suitably constructing the parameter R_F as as function of the orientation angle θ of the colliding nuclei. These properties of our formulation can be used to analyse fusion data within the concept of 'distribution of barriers' as outlined in [21, 25]. In the present set of numerical calculations we did not find it essential to incorporate this additional degree of

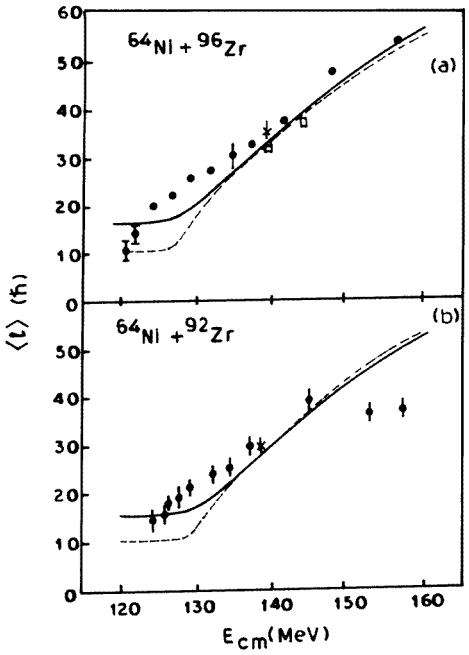

Figure 5. Variation of $\langle l \rangle$ as a function of $E_{\rm cm}$ for ^{64}Ni + ^{92,96}Zr. The full curves represent the results of the present calculation. The experimental data (full dots) and the broken curves representing CC results have been taken from [5].

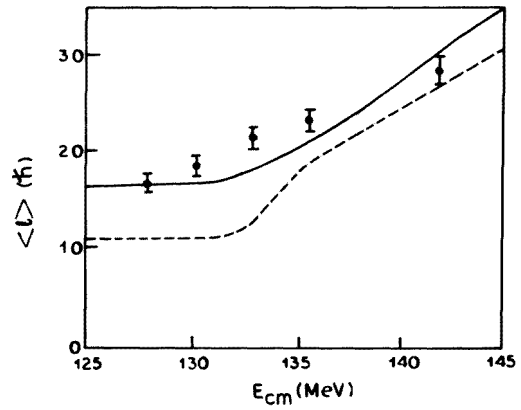

Figure 6. Same as figure 5 for ^{64}Ni + ^{100}Mo. The full curve represents results of the present calculation. The experimental data (full dots) and the CC results (broken curve) are obtained from [3].

freedom, even though we do not rule out the necessity of considering this in the other cases of fusion process involving highly deformed nuclei.

4. Summary and conclusions

We now summarize the main observations and conclusions of the present paper. Based on the concept of the EFB model [11] and unified formulae of transmission coefficients adopting the procedure of [14], general expressions for transmission coefficients T_l in the lth partial wave at $E_{\rm cm}$ both below and above the Coulomb barrier are derived. The partial-wave expansion of $\sigma_{\rm F}$ through these T_l is then integrated over l to give closed formulae for $\sigma_{\rm F}$ as a function of $E_{\rm cm}$. Subsequently, the results of mean spin $\langle l \rangle$ are obtained from these expressions of $\sigma_{\rm F}$. The formulation is applied to several nucleus–nucleus systems namely ^{64}Ni + ^{92,96}Zr, ^{64}Ni + ^{100}Mo and ^{16}O + ^{166}Er involving both heavy and light nuclei. The fits to the experimental $\sigma_{\rm F}$ and $\langle l \rangle$ data are found to be quite good in general. In particular, in the cases of ^{64}Ni + ^{92,96}Zr and ^{64}Ni + ^{100}Mo, unlike the CC calculations and Wong formula [5], we find that our results of $\sigma_{\rm F}$, $\sigma_{\rm F}^{l}$ and $\langle l \rangle$ explain the corresponding experimental results reasonably well both in the below- and above-barrier energy region.

Acknowledgments

We thank Professor C R Praharaj for valuable discussions. We are grateful to the Director, Nuclear Science Center, New Delhi for the facilities provided to us for the completion of part of this work. Thanks are due to Mr K K Nanda and Mr B B Dhal for useful discussions and help in preparing the manuscript. One of us (BS) gratefully acknowledges the research facilities extended to him by the Institute of Physics, Bhubaneswar and Indira Gandhi Institute of Technology, Sarang.

References

[1] Beckerman M 1985 *Phys. Rep.* **129** 145
[2] Steadman S G and Rhoades-Brown M J 1986 *Ann. Rev. Nucl. Part. Sci.* **36** 649
[3] Halbert M L *et al* 1989 *Phys. Rev.* C **40** 2558
[4] Gil S *et al* 1990 *Phys. Rev. Lett.* **65** 3100
[5] Stefanini A M 1992 *Nucl. Phys.* A **538** 195c
[6] Ishihara M, Takigawa N and Yamaji S 1993 *Proc. Workshop on Heavy-Ion Reactions with Neutron Rich Beams (Wako, Japan)* (Singapore: World Scientific)
[7] Dasso C H and Landowne S 1987 *Comp. Phys. Comm.* **46** 187; 1987 *Phys. Lett.* **183B** 141
[8] Rhoades-Brown M J *et al* 1980 *Phys. Rev.* C **21** 2417, 2436
[9] Hill D L and Wheeler J A 1953 *Phys. Rev.* **89** 1102
[10] Wong C Y 1973 *Phys. Rev. Lett.* **31** 766
[11] Sahu B and Shastry C S 1989 *J. Phys. G: Nucl. Phys.* **15** L149; 1990 *J. Phys. G: Nucl. Phys.* **16** 55; 1989 *Proc. Int. Seminar on Direct Nuclear Reactions (Bangalore)* ed N G Puttaswamy (Bangalore: Indian Academy of Sciences) p 139
[12] Udagawa T, Kim B T and Tamura T 1985 *Phys. Rev.* C **32** 124
[13] Kubo K-I, Manyum P and Hodgson P E 1991 *Nucl. Phys.* A y**534** 393
[14] Farina J E G 1988 *J. Phys. A: Math. Gen.* **21** 2547
[15] Satchler G R, Nagarajan M A, Lilley J S and Thompson I J 1987 *Ann. Phys., NY* **178** 110
[16] Marten J and Fröbrich P 1992 *Nucl. Phys.* A **545** 854
[17] Kittl J A and Testoni J E 1986 *Nucl. Phys.* A **453** 162
[18] More R M and Warren K H 1991 *Ann. Phys.* **207** 282
[19] Spanier J and Oldham K B 1987 *An Atlas of Functions* (New York: Hemisphere)
[20] Broglia R A and Winther A 1981 *Heavy-Ion Reactions Lecture Notes* vol 1 (Redwood City, CA: Addison-Wesley) p 116
[21] Rowley N, Satchler G R and Stelson P H 1991 *Phys. Lett.* **254B** 25
[22] Takigawa N, Sagawa H and Shinozuka T 1992 *Nucl. Phys.* A **538** 221c
[23] Denisov V Yu and Royer G 1994 *J. Phys. G: Nucl. Part. Phys.* **20** L43
[24] Denisov V Yu and Royer G 1995 *Phys. Atom. Nucl.* **58** 397
[25] Stefanini A M *et al* 1995 *Phys. Rev. Lett.* **74** 864